J. Chem. Sci. Vol. 124, No. 1, January 2012, pp. 291–300.

On the nature of highly vibrationally excited states of thiophosgene[#]

SRIHARI KESHAVAMURTHY
Department of Chemistry, Indian Institute of Technology Kanpur, Kanpur 208 016, India
e-mail: srihari@iitk.ac.in

Abstract. In this work an analysis of the highly vibrationally excited states of thiophosgene ($SCCl_2$) is made in order to gain insights into some of the experimental observations and spectral features. The states analysed here lie in a spectrally complex region where strong mode mixings are expected due to the overlap of several strong anharmonic Fermi resonances. Two recent techniques, a semiclassical angle space representation of the eigenstates and the parametric variation of the eigenvalues (level-velocities) are used to identify eigenstate sequences exhibiting common localization characteristics. Preliminary results on the influence of highly excited out-of-plane bending modes on the nature of the eigenstates suggest a possible bifurcation in the system.

Keywords. Thiophosgene; IVR; resonances; assignment; semiclassical.

1. Introdution

Understanding the nature of the highly excited molecular eigenstates is equivalent to deciphering the mechanism of intramolecular vibrational energy redistribution (IVR) occurring in the molecule.[1] However, the assignment of eigenstates is far from simple. The existence of and interplay of several strong anharmonic resonances result in complicated spectral patterns and highly mixed states. Nevertheless, eigenstates of molecular systems rarely exhibit the extreme scenario of being completely ergodic or completely regular.[2] A generic situation, even at fairly high energies, is the co-existence of several classes of eigenstates with differing degree of mixing being interspersed among each other.[3,4] More interestingly, the interspersed states can show several sequences associated with certain identifiable common localization characteristics. In other words, although a full set of quantum numbers do not exist for labelling such states, there are reasons to believe that a sufficient number of approximate quantum numbers do exist to understand, and hence assign, the eigenstates. Since the approximate quantum numbers arise out of the local dynamics due to specific resonances, relevant at the energies of interest, the assignment is inherently dynamical in nature. In a nutshell, several decades of work have shown that dynamical assignments can be done reliably only if the structure of the corresponding classical phase space is well-understood.[5]

This work is concerned with the dynamical assignment of the eigenstates of thiophosgene $SCCl_2$. The Hamiltonian of interest is a highly accurate spectroscopic Hamiltonian obtained[6] by Gruebele and Sibert via a canonical Van Vleck perturbation analysis of the experimentally derived normal mode potential surface.[7] The Hamiltonian can be expressed as $H = H_0 + V_{\rm res}$ with

$$\begin{aligned} H_0 &= \sum_i \omega_i \left(v_i+\frac{1}{2}\right)+\sum_{ij} x_{ij}\left(v_i+\frac{1}{2}\right)\left(v_j+\frac{1}{2}\right) \\ &\quad +\sum_{ijk} x_{ijk}\left(v_i+\frac{1}{2}\right)\left(v_j+\frac{1}{2}\right)\left(v_k+\frac{1}{2}\right), \\ V_{\rm res} &= K_{526}a_2^\dagger a_5 a_6^\dagger + K_{156}a_1 a_5^\dagger a_6^\dagger \\ &\quad +K_{125}a_1^\dagger a_2^\dagger a_5^2 + K_{36}a_3^2 a_6^{\dagger 2} \\ &\quad +K_{231}a_1^\dagger a_2 a_3^2 + K_{261}a_1^\dagger a_2 a_6^2 + \text{c.c.} \end{aligned} \tag{1}$$

The zeroth-order anharmonic Hamiltonian is H_0, whose eigenstates are the feature states and $V_{\rm res}$ accounts for the important anharmonic resonances responsible for the IVR dynamics. In the rest of the paper the various resonances will be refered to by simply indicating the modes. For instance, the first resonance term in $V_{\rm res}$ above will be refered to as the 526-resonance. The Hermitian adjoints of the operators are denoted by c.c., and the operators a_k, $a_k^\dagger$, and $v_k \equiv a_k^\dagger a_k$ are the lowering, raising, and number operators for the $k^{\rm th}$ mode, respectively with $[a_k, a_k^\dagger] = 1$, in analogy to the usual harmonic oscillator operators. Based on the possible resonances suggested by the normal mode frequencies and the observed spectral 'clumps' in the dispersed fluorescence spectra, three approximately

[#]Dedicated to Prof. N Sathyamurthy on his 60th birthday

conserved quantities (known as polyads) arise which can be expressed as

$$\begin{aligned} K &= v_1 + v_2 + v_3, \\ L &= 2v_1 + v_3 + v_5 + v_6, \\ M &= v_4. \end{aligned} \tag{2}$$

Thus, the ν_4 mode is not involved in any resonant interactions with the rest of the modes. Due to the polyad constraints one has effectively a three degree of freedom system and three of the quantum numbers out of a total six needed to assign a quantum state are already known. Nevertheless, as will be seen below, even this reduced system presents a stiff challenge with regards to the dynamical assignments of the highly excited eigenstates.

The IVR dynamics in $SCCl_2$ has been the subject of several recent experimental[7–9] and theoretical[10–12] studies. In an early detailed study, Strickler and Gruebele established[7] that the IVR state space (zeroth-order quantum number space) has an effective dimensionality of three as opposed to the theoretically possible six. Combined with the observation of regular progressions persisting up to the first dissociation energy of about 600 THz, one expects restricted IVR in the system. This in itself is surprising since the effective Hamiltonian fit, as in equation 1, to the stimulated emission pumping (SEP) spectra contains strong multimode Fermi resonances. In addition, the SEP spectra are quite complex and congested in the 200–300 THz region. However, it was noted that the regular progressions mainly involved the Franck–Condon active ν_1 (C–S stretch) and the ν_4 (out-of-plane bend) modes, and thus avoided the strongest resonances. Furthermore, Chowdary and Gruebele recently[8] showed the existence of sharp SEP spectral features in the energy range of 550–700 THz which includes both the molecular $SCCl_2 \rightarrow CS + Cl_2$ and the radical $SCCl_2 \rightarrow SCCl + Cl$ dissociation channels. Although, one could rationalize the observation as due to the avoidance of the strong 526-resonance involving modes ν_2 (a_1 symmetry C–Cl stretch), ν_5 (b_2 symmetry C–Cl stretch), and ν_6 (b_2 symmetry Cl–C–Cl bend), a similar argument for the equally strong 156-resonance involving modes ν_1 (a_1 symmetry C=S stretch), ν_5, and ν_6 is not possible. Sibert and Gruebele performed[6] a detailed study of the IVR dynamics using equation 1 and concluded that around 240 THz ($\sim$ 8000 cm^{-1}), close to the threshold for facile IVR, zeroth-order states coexist exhibiting a broad range of dynamical behaviour ranging from fairly restricted to highly facile IVR. A rather extensive study[10] of nearly 10^6 zeroth-order bright ('feature') states by Chowdary and Gruebele concluded that about one in thousand feature states are localized even at the highest energy — not enough to invalidate statistical theories but certainly indicating that even near the dissociation limit $SCCl_2$ is not just a bag-of-atoms.

The above observations hint at the existence of different classes of eigenstates in a specific energy range. For instance, even around an energy of about 590 THz one observes[8] states whose IVR line widths vary non-monotonically with energy. Thus, in order to gain further insights into the IVR dynamics a closer look at the eigenstates of equation 1 is necessary. An earlier work by Jung, Taylor, and Sibert using a second order version of equation 1 established[11] that several distinct eigenstate classes exist in the spectrally complicated region 7000–9000 cm^{-1} ($\sim$ 210–270 THz). More recently,[12] Jung and Taylor dynamically assigned the states and came up with a detailed semiclassical classification scheme for the eigenstates.

In this work, an attempt is made to answer the following questions. Firstly, can one identify the various eigenstate classes in a manner that is not dependent on visualizing the high dimensional wavefunctions quantum mechnically or semiclassically? More importantly, such a method should be able to make contact with the relevant structures like periodic orbits and their bifurcations in the high dimensional classical phase space. Secondly, do the eigenstate classes and sequences identified previously persist when using a higher order and more accurate Hamiltonian? Finally, is there a possibility of new modes being born due to specific bifurcations in the system?

1.1 *Classical limit Hamiltonian*

In order to dynamically assign the eigenstates it is important to analyse the classical limit Hamiltonian corresponding to equation 1 and the procedure is well-established in literature. The full classical Hamiltonian, in terms of the zeroth-order action-angle variables $(\mathbf{I}, \boldsymbol{\theta})$, can be found in an earlier work.[11] Here, the reduced three degree of freedom classical Hamiltonian, taking into cognizance of the polyads (K, L, M), is of interest and can be obtained via a suitable $(\mathbf{I}, \boldsymbol{\theta}) \rightarrow (\mathbf{J}, \boldsymbol{\psi})$ canonical transformation.[11] The resulting reduced Hamiltonian can be expressed as $H(\mathbf{J}, \boldsymbol{\psi}) = H_0(\mathbf{J}) + V_{\rm res}(\mathbf{J}, \boldsymbol{\psi})$ where,

$$\begin{aligned} H_0(\mathbf{J}, \boldsymbol{\psi}) &= C + \sum_{i=1}^{3} \varpi_i J_i + \sum_{i,j=1}^{3} \alpha_{ij} J_i J_j \\ &+ \sum_{i,j,k=1}^{3} \beta_{ijk} J_i J_j J_k, \end{aligned} \tag{3}$$

is the zeroth-order Hamiltonian and the resonant perturbations (nonlinear resonances) are given by

$$\begin{aligned} V_{\rm res}(\mathbf{J},\boldsymbol{\psi}) &= v_{156}(\mathbf{J};K_c,L_c)\cos\psi_1 \\ &+ v_{526}(\mathbf{J};K_c,L_c)\cos\psi_2 \\ &+ v_{125}(\mathbf{J};K_c)\cos(\psi_1+\psi_2) \\ &+ v_{36}(\mathbf{J};K_c,L_c)\cos 2\psi_3 \\ &+ v_{231}(\mathbf{J})\cos(\psi_1-\psi_2-2\psi_3) \\ &+ v_{261}(\mathbf{J};K_c,L_c)\cos(\psi_1-\psi_2). \quad (4) \end{aligned}$$

In the above equations the actions conjugate to the angles (ψ_4,ψ_5,ψ_6) are $(K_c = K+3/2, L_c = L+5/2, M_c = M+1/2)$ i.e., the classical analogs of the quantum polyads. The transformed actions $\{J_k\}$ are related to the zeroth-order quantum numbers as $J_k = (v_k+1/2)\hbar$. The various parameters $(C,\boldsymbol{\varpi},\boldsymbol{\alpha},\boldsymbol{\beta})$ of the reduced Hamiltonian are determined in terms of the original parameters (see supplementary information in reference 6 for the values). The relations are not shown here but note that at this order the parameters $(C,\boldsymbol{\varpi},\boldsymbol{\alpha})$ depend on the polyads K, L, and M.

2. Dynamical assignment

In this section, two recent techniques,[13,14] used to analyse the highly excited eigenstates, are briefly mentioned. The reader is referred to an earlier publication[16] for the theoretical basis and validity of the methods along with a detailed comparison.

In the first approach[11–13] the quantum states $|\alpha\rangle$ for a given (K,L,M) are expressed in the semiclassical angle space $\boldsymbol{\psi} = (\psi_1,\psi_2,\psi_3)$ as

$$\langle\boldsymbol{\psi}|\alpha\rangle = \sum_{\mathbf{v}\in(K,L,M)} C_{\alpha\mathbf{v}}e^{i\mathbf{v}\cdot\boldsymbol{\psi}}, \quad (5)$$

with $\mathbf{v} = (v_1,v_2,v_3)$ and ignoring an overall phase factor. Due to the 2π-periodicity of the angles, the semiclassical wavefunctions $\alpha(\boldsymbol{\psi})$ now 'live' on the classical reduced configuration space which is a three-dimensional torus T^3. The nature of the states is determined by plotting the density $|\langle\boldsymbol{\psi}|\alpha\rangle|^2$ and the phase of equation 5 on select two-dimensional sections of T^3.

The second approach[14,16] involves computing the eigenstate expectation values of the various anharmonic resonances. The expectation values are naturally related to the parametric variation of the corresponding eigenvalues, also called as the level-velocities. For example,

$$\langle\alpha|\hat{V}_{156}|\alpha\rangle = \frac{\partial E_\alpha}{\partial K_{156}}. \quad (6)$$

Previous works[14–17] have shown that the level-velocities, semiclassically, are extremely sensitive to the underlying structures in the classical phase space. There is also an interesting connection (not elaborated here) between the parametric variation of eigenvalues and the matrix fluctuation-dissipation theorem[18] of Gruebele. In what follows the terms expectation values and level-velocities will be used interchangeably.

Recently[16] it was argued that a combination of the above approaches can be very powerful towards gaining key insights into the nature of the highly excited eigenstates. The current work provides further support for such an argument. To begin with, a single resonance case is analysed in order to set the stage for looking at select eigenstates of the full system. Although the single resonance case is classically integrable, the correct assignment of the states needs to be done with care due to the multimode nature of the resonance.

2.1 *Integrable multimode resonance*

In the full quantum Hamiltonian, all the anharmonic resonances as shown in in equation 1 are turned off except for the multimode 156-resonance. Since, the quantum and classical Hamiltonians couple only the ν_1, ν_5, and ν_6 modes, the quantum numbers (v_2,v_3) are good quantum numbers. Consequently, one already has five good quantum numbers (K,L,M,v_2,v_3) to label those quantum states that are under the influence of the said resonance. States that are not affected by the resonance are trivially assigned by the full set of zeroth-order quantum numbers and hence will not be discussed further. In the present case it is desirable to organize the states using $P_s \equiv (L-v_3)$ since this represents the plane on which the states live in the original six-dimensional state space.

The geometry of the (v_1,v_5,v_6) space is shown in figure 1 for the specific case of $v_3 = 0$. For given (K,L,M), the space is filled with P_s-planes with v_3 being fixed on each plane. On a given P_s-plane, fixed values of v_2 correspond to lines determined by points $(v_1, K_2-v_1, P_s-K_2-v_1)$ with $K_2 \equiv K-v_2$. An eigenstate will be delocalized only along one of the lines on the P_s-plane. Two points are to be noted at this stage. Firstly, the area of the P_s-planes decrease with increasing v_3 and the length of the lines on a given plane decreases with increasing v_2. Consequently, unperturbed normal modes should be expected for high excitations in the (v_2,v_3) modes. Secondly, the number of state space points $(v_1, K_2-v_1, P_s-K_2-v_1)$ on a given line determines the quantum number μ, an

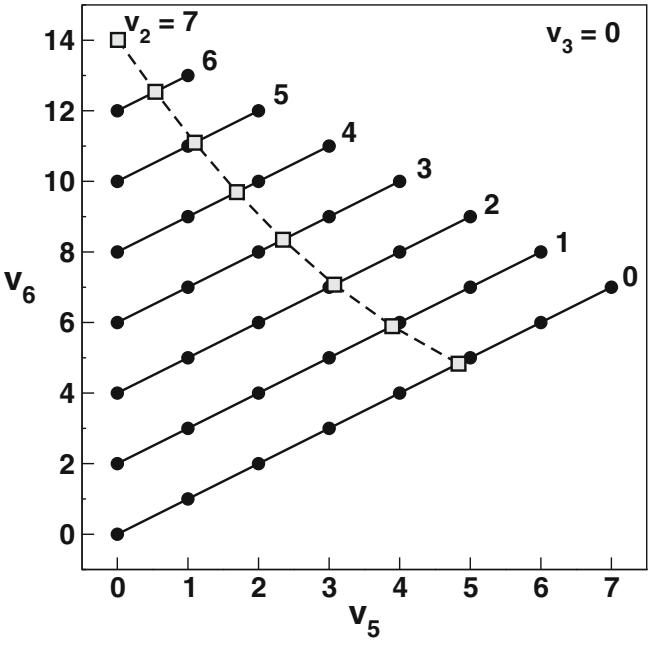

Figure 1. Projection of the $P_s = 14$ plane onto the (v_5, v_6) space. Mixing of the zeroth-order states occurs only along lines corresponding to constant values of v_2 (indicated) leading to the sequences observed in figure 2a and b. Classical prediction (cf. equation 8, grey squares) of the maximal level-velocities corresponding to large quantum eigenstate expectation value $\langle \hat{V}_{156} \rangle$ of the 156-resonance operator.

excitation index, related to the phase space area enclosed by the 156-resonance island in the classical phase space.

Therefore, a knowledge of the quantum number μ provides a complete assignment $|K, L, M, P_s; v_2, \mu\rangle$ of the single resonance eigenstates. This information can be obtained both from the semiclassical wavefunction and the level-velocity approaches mentioned above. For instance, looking at the phase of the semiclassical state in the $\psi_1 = 0$ plane will immediately reveal the (v_2, v_3) quantum numbers. Similarly, keeping track of the phase advance along the ψ_1 direction in the $\psi_3 = 0$ or $\psi_2 = 0$ plane will yield μ as the excitation quantum number.[12,13]

Equivalently, in figure 2a the quantum eigenstate expectation values of the 156-resonance operator are shown. The apparent congested nature of the figure is a direct result of the interleaving of the various state sequences with different v_3. The sequences, however, can be easily identified by analysing the corresponding classical phase space function $v_{156}(\mathbf{J}; K_c, L_c) \cos \psi_1$ with

$$v_{156} \equiv 2\,[J_1(K_{2c} - J_1)(P_{sc} - K_{2c} - J_1]^{1/2}\,. \qquad (7)$$

In the above expression, the quantities K_{2c} and P_{sc} correspond to the classical analogs of the quantum K_2 and P_s, respectively. It can be shown that classical expectation value is large and has equal magnitudes at the resonant angles $\bar{\psi}_1 = 0, \pi$ and resonant action

$$\bar{J}_1 = \frac{1}{3}\left[P_{sc} - \sqrt{P_{sc}^2 - 3K_{2c}(P_{sc} - K_{2c})}\right]. \qquad (8)$$

The expectation values are positive for $\psi_1 = 0$ and negative for $\psi_1 = \pi$. From the classical phase space perspective the opposite signs translate to states being localized about the stable or unstable fixed points of the resonance island. Using the classical estimate it is possible to identify the highly localized states which further spawn the sequences with different μ and in figure 2b some of the v_2-sequences for fixed $v_3 = 0$ i.e., $P_s = 14$ are shown. For instance, the sequence shown in figure 2b (circles) is assigned as $|7, 14, 0, 14; 0, \mu\rangle$ with $\mu = 0$ (maximum positive expectation value) to $\mu = 7$ (maximum negative expectation value). All such sequences can be easily identified and hence a complete assignment of the integrable, single resonance cases can be provided in terms of the appropriate quantum numbers.

Including other independent resonances in equation 1 results in a non-integrable system with highly mixed states which are presumably interspersed with some of the regular states. For example, including the 526-resonance (and/or the 125-resonance) in addition to the 156-resonance destroys the v_2 quantum number. In terms of the geometry described above, since v_3 is still conserved, the P_s-planes are preserved but the states now spread over the entire plane. Further inclusion of the 231-resonance and 36-resonance destroys the P_s-planes as well and the states now spread over the entire state space. In the next two sections the goodness of v_2 and v_3 are broken sequentially in order to check if any new state sequences appear despite the non-integrability of the system.

2.2 *Breaking the goodness of* v_2

In this section only the resonances involving modes ν_1, ν_2, ν_5, and ν_6 are considered. Thus, v_2 is no longer a good quantum number whereas v_3 is still a good quantum number. Note that the set of resonances involved here are the strongest ones in thiophosgene and therefore strong state mixings are expected. Are there any patterns in this case? In analogy to figure 2b, the $v_3 = 0$ case of the nonintegrable system is shown in figure 3 using the level velocity approach. Since several level

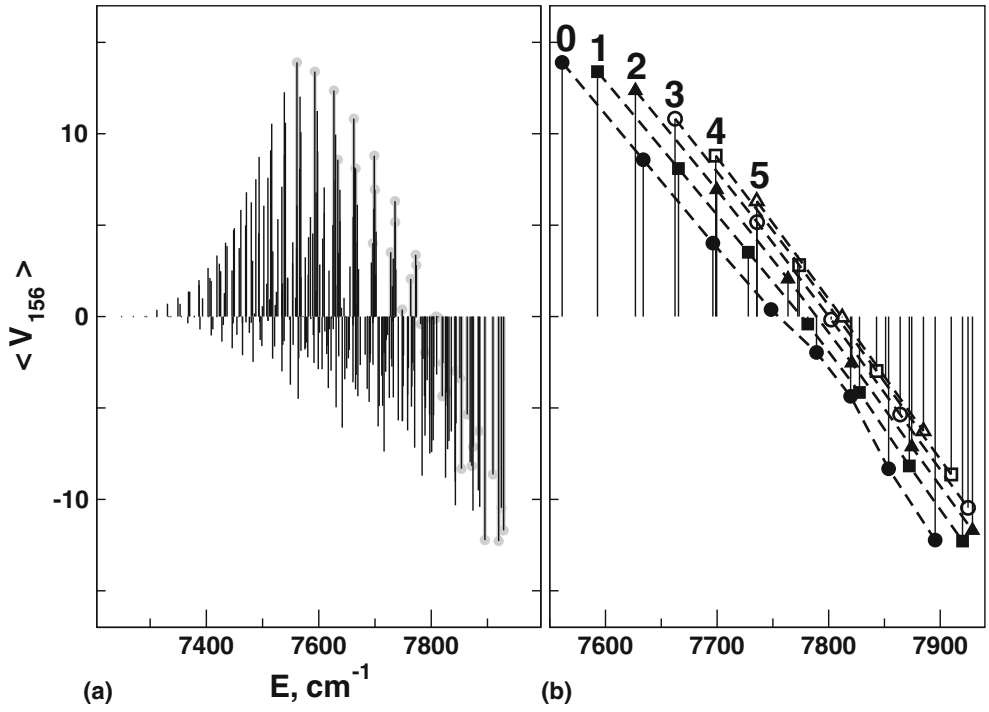

Figure 2. Single 156-resonance Hamiltonian. (**a**) Quantum expectation values $\langle V_{156}\rangle$ as a function of the eigenenergies. The apparent complexity is due to the interspersing of several easily identifiable regular sequence of states. (**b**) $\langle V_{156}\rangle$ for states with $v_3 = 0$, i.e., $P_{156} \equiv 2v_1 + v_5 + v_6 = 14$ (also shown in (**a**) as grey circles). Various sequences with differing v_2 are indicated by dashed lines. A sequence corresponding to say $v_2 = 0$ (filled circles) is assigned as $|7, 14, 0, 14; 0, \mu\rangle$ with $\mu = 0, 1, \ldots, 7$ being an excitation index. See text for explanations.

velocities are compared in the figure, all of them are scaled to zero mean and unit variance.

From figure 3, it is clear that eigenstate sequences do exist in this non-integrable case and a few of them are highlighted by dashed lines. It is important to note that the observed sequences are different from the v_2-sequences seen in figure 2b since v_2 is no longer a good quantum number. Three key observations are worth making at this stage. Firstly, the initial sequences starting at high energy can be identified using $\langle V_{156}\rangle$ or equally well using $\langle V_{526}\rangle$, two of the strongest resonances in the system. Interestingly, as evident from figure 3(top inset), these sequences can also be identified from $\langle V_{125}\rangle$ and $\langle V_{261}\rangle$ values. The large values of $\langle V_{261}\rangle$ despite the weakness of the 261-resonance is an example of the non-trivial nature of such multiresonant systems. The two major resonances induce a relatively strong 261-resonance in certain regions of the P_s plane, resulting in significant perturbation of the state sequences. Thus, at high energies the states are under the influence of several resonances. Secondly, at low energies the sequences are less robust (note the curvature of the dashed lines in the figure) and fewer in number, but seem to be organized more by the 526-resonance. Thirdly, the various sequences 'collide' near $E \sim 7800\ \text{cm}^{-1}$ leading to significant disruption of the regularity of the sequences. Small level velocities and energy spacings in this region imply several multistate avoided crossings and suggest that the state mixing could be due to dynamical tunneling.[19] Dynamical assignments of the states in this complicated transition region are difficult if not impossible.

Support for the level velocity predictions comes from computing the participation ratio N_P in the various single resonance basis $|\mathbf{r}\rangle$ (eigenstates of single resonance Hamiltonians), shown in figure 3(bottom inset). The number of basis states participating in a given eigenstate $|\alpha\rangle$ is computed as

$$N_P = \left(\sum_{\mathbf{r}} |\langle \mathbf{r}|\alpha\rangle|^4\right)^{-1}. \tag{9}$$

The participation ratios indicate that, except for a few states at the high and low energy ends, most states are moderately mixed. Moreover, large values of N_P at $E \sim 7800\ \text{cm}^{-1}$ in every basis agrees well with the level velocity data. Note that hints for the existence of eigenstate sequences are present in the N_P data, but nowhere

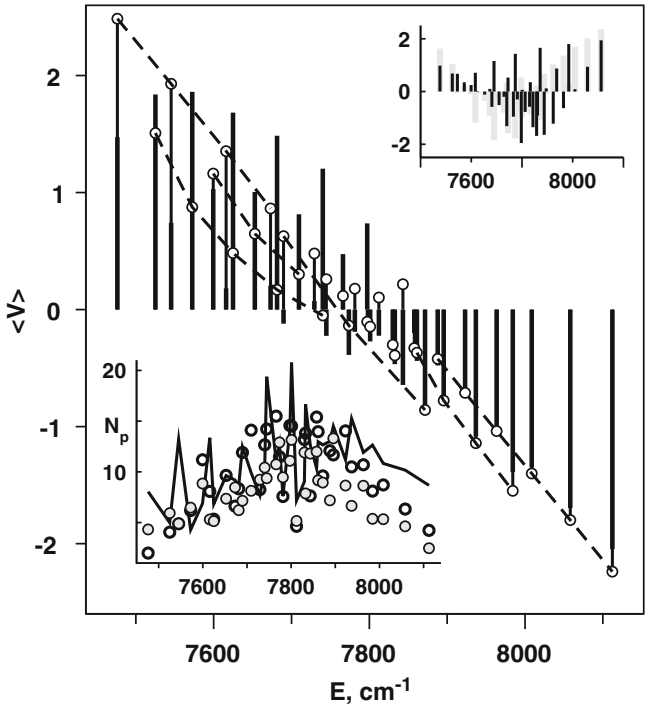

Figure 3. Scaled level velocities for the noninetgrable system with 156 (thick black lines), 526 (thin lines with open circles), 125 (black lines in top inset), and the 261 (grey lines in top inset) anharmonic resonances present. Eigenstates belonging to the good quantum number $v_3 = 0$ are shown. Two eigenstate sequences (dashed lines) starting at the high energy end are easily identified. Similar sequences at the low energy end are also shown. The sequences merge towards the middle resulting in mixed states. (Bottom inset) Participation ratios N_p (cf. equation 9) in the 156 (grey circles), 526 (black open circles), and 125 (black line) single resonance basis.

as emphatically as reflected in the level velocity plots.

The various sequences observed here are consistent[12] with the previous results of Jung and Taylor. This can be established by looking at appropriate slices of the semiclassical three-dimensional angle space representations of the eiegnstates. In figure 4 the semiclassical $(\psi_1, \psi_2; \psi_3 = 0)$ angle space representations are shown for select states in the $v_3 = 0$ manifold. A striking correspondence can be seen between the sequences revealed by the level velocities shown in figure 3 and the eigenstate density patterns as observed in the semiclassical angle space. The first column of states correspond to the sequence, indicated in figure 3, starting with the highest energy state and have clear nodal structure — no nodes in the diagonal direction and increasing number of nodes in the antidiagonal direction. Similarly, states in the second column belong to the second high energy sequence indicated in figure 3 and exhibit an additional node in the diagonal direction. Both these sequences correspond to the class A classification given earlier[12] and the nodes along the diagonal and antidiagonal directions yield two additional quantum numbers t_d and t_a, respectively. For instance, the first state in column one of figure 4 is assigned as $|K, L, M; v_3 = 0, t_d = 0, t_a = 0\rangle$ and the assignment $|K, L, M; 0, 1, 2\rangle$ is appropriate for last state in the second column.

On the other hand, the third column in figure 4 corresponds well to the sequence indicated in figure 3 starting with the lowest energy state. Although the angle space densities show localization around $\psi_1 = 0, 2\pi$, suggesting 156-resonant states, the level velocity results show that the influence of the 526-resonance is far greater in comparison. State space plots and the participation ratio data do establish the first state of the sequence to be closer to being a 526-resonant state. However, the later states in the sequence are perturbed strongly by the induced 261 resonance (see the top inset of figure 3) and hence non-trivial to assign. The last column of figure 4 show three states that are in the complicated energy region around 7800 cm^{-1}. The mixed nature of these states is evident both from the angle space densities as well as the level velocity and participation ratio data. Presumably the induced 261-resonance is leading to the highly mixed states. In particular, the middle state of the last column seems to be a state that is delocalized over an extended region of the phase space and such states have been observed in a different context in an earlier study.[16]

2.3 *Breaking the goodness of v_3 - the full system*

The previous section identified sequences of eigenstates exhibiting similar localization properties of a subsystem of the full Hamiltonian equation 1, wherein v_3 was a good quantum number. The goodness of v_3 is strictly broken in the full system, obtained from the subsystem with the inclusion of the remaining 36-and the 231-resonances. A key question is whether the sequences in figure 3 would persist in the full system. The answer to this question can be obtained by analysing figure 5 which shows scaled $\langle V_{156}\rangle$ and $\langle V_{526}\rangle$ for all the 288 eigenstates. The expectation values $\langle V_{261}\rangle$ and $\langle V_{125}\rangle$ are also substantial, as in figure 3, but not shown for the purpose of clarity. It is immediately clear from figure 5 that the high end of the polyad does exhibit several sequences highlighted by solid and dashed lines connecting the states. Specifically, the solid line sequences correspond to increasing v_3 with fixed (t_d, t_a) quantum numbers and the dashed lines correspond to increasing t_d with $t_a = 0$ and fixed v_3 values. In

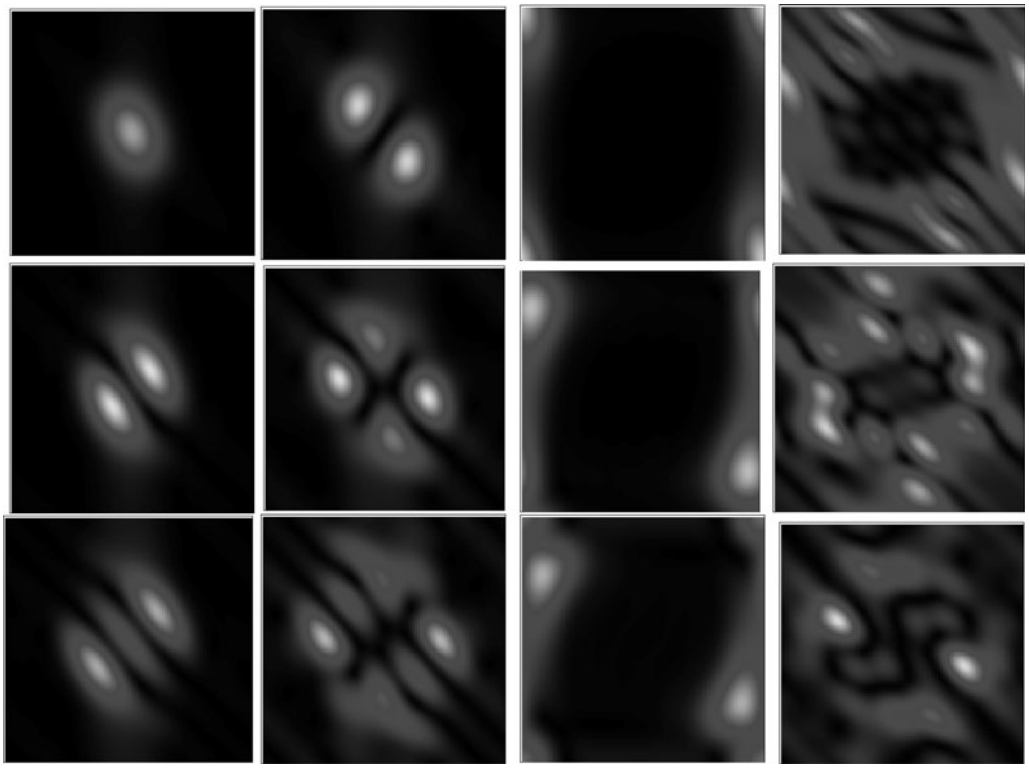

Figure 4. Semiclassical (ψ_1, ψ_2) angle space representations of select states corresponding to the case shown in figure 3 with $v_3 = 0$ being a good quantum number. The $\psi_3 = 0$ slice of the full three-dimensional space are shown. In every plot the angles range from 0 to 2π. (First column) States belonging to the first sequence in figure 3 starting at the highest energy. (Second column) States forming the second sequence in figure 3 at high energy. (Third column) States belonging to the first sequence in figure 3 starting at the lowest energy. (Last column) States that do not form any clear sequence. See text for discussions.

particular, these high energy states correspond precisely to the class A states discussed in the previous section with similar semiclassical (ψ_1, ψ_2) angle space representations. Note that in figure 3 only the $v_3 = 0$ states are shown and including states for different values of v_3 would show high energy patterns similar to those seen in figure 5.

The robustness of the class A sequences is also confirmed in figure 5a wherein the participation ratio of the high energy eigenstates is seen to be nearly unity in the v_3-good basis i.e., in the eigenbasis of the subsytem discussed in the previous section. For these set of states v_3 is approximately conserved and can be used to label the eigenstates. Consequently, it is possible to infer that the lowest frequency mode ν_3 (a_1, Cl–C–Cl bend) is decoupled from the rest of the modes in the $[7800, 8100]$ cm^{-1} region. The IVR dynamics ensuing from a feature (anharmonic zeroth order) state comprising mainly of the class A states is therefore expected to be non-statistical. A crucial observation in this context is summarized in figure 5b - participation ratios in the zeroth-order basis are unable to identify the various sequences as reflected in the expectation value patterns. Stated differently, delocalization in state space does not immediately imply delocalization in the semiclassical angle space and hence in the full phase space.

Furthermore, two important observations can be made in the mid to low energy regions of the polyad. Firstly, for $E \lesssim 7800$ cm^{-1} it is clear from figure 5a that the goodness of v_3 is broken substantially. Indeed, the regular lattice formed by the various sequences at the high energy end of the polyad begins to 'dissolve' around $E \sim 7800$ cm^{-1} due to the influence of several resonances. Secondly, at the lowest energy end, the states are mainly influenced by the 526-resonance and hence, as noted earlier, typical class C states. The middle region of the polyad spanning $[7350, 7750]$ cm^{-1} is particularly complicated with several highly mixed states and states exhibiting transitional nature between the two extreme classes, A and C, of localized states.

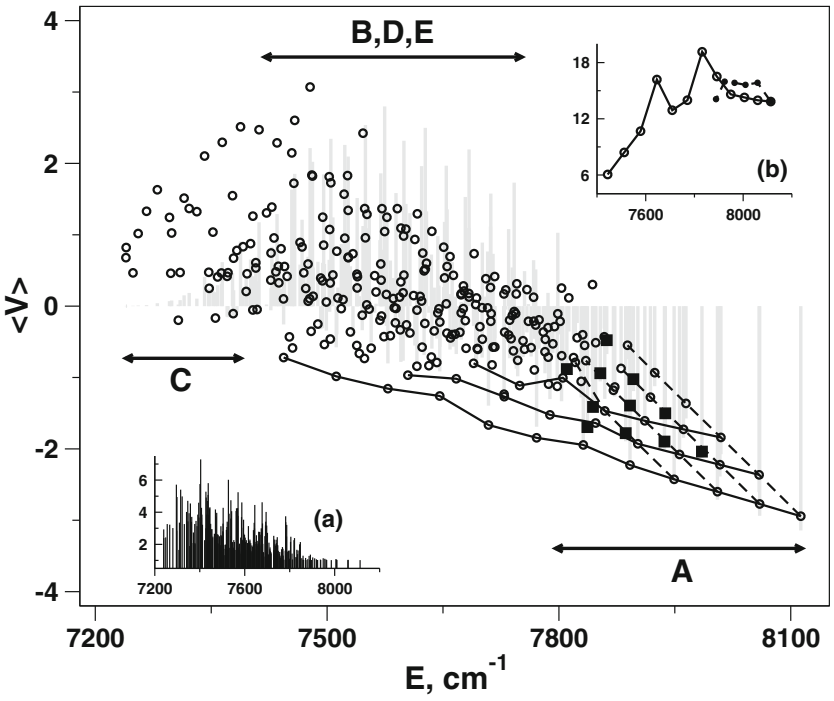

Figure 5. Eigenstate sequences as revealed by $\langle V_{156}\rangle$ (in grey) and $\langle V_{526}\rangle$ (circles) forthe full Hamiltonian. The various classes of eigenstates are denoted by A,B,C,D, and E in accordance with an earlier study.[12] Sequences with increasing v_3 with fixed (t_d, t_a) (black lines). Sequences with increasing t_d with $t_a = 0$ and fixed v_3 (dashed lines). States with varying v_3, t_d and fixed $t_a = 1$ (squares). (**a**) Participation ratio of the eigenstates in the v_3-good basis. Note the significant breakdown of the goodness of v_3 in the middle of the polyad. (**b**) Participation ratio in the zeroth-order basis of the $(t_d, t_a) = (0, 0)$ sequence (solid line) and $v_3 = 0$ sequence (dashed lines).

3. Highly excited v_4 states

Up until now the focus has been exclusively on the $v_4 = 0$ case i.e., no excitations in the out-of-plane bending mode. Experimentally, however, the ν_1 and ν_4 modes have dominant Franck–Condon activity[7] and sharp assignable features in the spectra are seen[8] even around and above the dissociation energy. Most of the sharp features have fairly large values of v_4 in their assignments. Thus, it is interesting to ask if the nature of the eigenstates, in terms of localization as well as the different classes, undergo any significant change upon exciting the ν_4 mode. Earlier works have hinted at a smooth morphing of the reduced dimensional wavefunctions[8] with increasing ν_4 excitation and the existence of IVR-protected zeroth-order states for large number of quanta in the ν_4 mode.[6] Can the level-velocity technique used in this work provide any insights?

As a preliminary effort, figure 6 summarizes the result of increasing ν_4 excitation on the highest energy eigenstate in the polyads $[K = 7, L = 14, v_4]$. The total number of eigenstates remains the same (288) due to the decoupling of the ν_4 mode from the other modes, but the

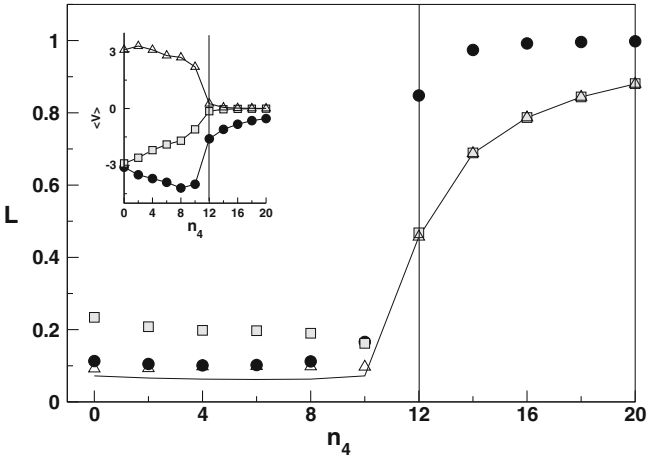

Figure 6. Variation of the participation ratios of the highest energy eigenstate in the polyad $[7, 14, v_4]$ with increasing excitation of the out-of-plane bending mode ν_4. The zeroth-order basis, 156, 526, and 125 single resonance basis values are shown as black line, filled circles, grey squares, and triangles, respectively. Inset shows the expectation values $\langle V_{156}\rangle$ (filled circles), $\langle V_{526}\rangle$ (grey squares), and $\langle V_{125}\rangle$ (triangles) for the highest energy state as a function of v_4. Note the sharp transition in both measures around $v_4 = 12$.

eigenstates span higher energy ranges. The main part of figure 6 shows the participation ratios of the eigenstate in various basis. Clearly, the highest energy state changes it nature from the one shown in figure 4 (first state of the first column) to one that is highly localized. Looking at the state space representation of the eigenstate for $v_4 = 20$ it becomes clear that it is a pure normal mode state. More importantly, the participation ratios undergo a sharp transition around $v_4 = 12$, signalling a significant change in the nature of the eigenstate. It is intriguing to observe that the 156-resonance basis value exhibits a much sharper transition as compared to the other basis.

The various scaled expectation values shown in the inset of figure 6 confirm the results based on the participation ratios. In particular, an equally sharp transtition is also seen in this case at $v_4 = 12$ and hence establishes the sensitivity of the level-velocities to the changing nature of the eigenstate. For $v_4 \geq 12$ all the expectation values are close to zero and thus predict a pure normal mode state. Incidentally, the results here agree well with the observation of IVR-protected zeroth-order states around $v_4 = 10$ in an earlier study[6] by Sibert and Gruebele (see figure 7 of their paper). However, it is interesting to note that the expectation values take on maximum values where the participation ratios are minimum. Similar observations[15] were made in an earlier study regarding the appearance of new modes in highly excited acetylene. Thus, the results of figure 6 suggest that there is a bifurcation in the underlying classical phase space which could be responsible for the experimental observation of sharp features near the dissociation threshold. Undoubtedly, more work is needed to establish the detailed bifurcation structure of the classical phase space and corresponding fingerprints on the quantum eigenstates. Perhaps, such an analysis would resolve the puzzle as to why such sharp features can be predicted[8] with an effective Hamiltonian without any resonance couplings.

4. Conclusions

The central point of this work is to emphasize the fact that highly excited eigenstates of multiresonant effective Hamiltonians form several sequences, corresponding to different classes of dynamics, interspersed amongst each other in a complicated fashion. However, the tools used in this work are ideal to disentangle the sequences and gain insights into the nature of the eigenstates. A remarkable aspect that emerges from this and other previous studies is worth noting — the expectation values shown, for example, in figure 5 are quantum objects. Nevertheless, the observed patterns and sequences in the expectation values have a one-to-one correspondence with the semiclassical angle space densities of the eigenstates. Thus, this establishes the close classical-quantum correspondence that exists for spectroscopic Hamiltonians. At the same time, the observation that state space based measures of localization or delocalization of the eigenstates are insufficient to identify the sequences suggests that phase space is the ideal setting where the true nature of the eigenstates are revealed — a conclusion that fortifies decades of earlier work[5] on systems with smaller degrees of freedom. The semiclassical action-angle representation is not all that abstract afterall!

It is heartening to see that the simple level-velocity approach is capable of identifying the eigenstate sequences. The present work agrees, to a large extent, with the previous analysis[12] and classification of the eigenstates. In particular, the eigenstate classes predicted in the earlier studies do persist in this study which uses a more accurate Hamiltonian. Therefore, the different classes of eigenstates and predictions of their influence on the IVR dynamics of certain zeroth-order bright states are expected to be robust even upon inclusion of other weak higher order resonances. The approach adopted in this work is easily generalized to systems with any number of degrees of freedom with several anharmonic resonances. The recently proposed method[16] of lifting the eigenstates onto the Arnold web i.e., the network of nonlinear resonances can lead to further detailed insights into the anatomy of certain mixed states (cf. last column of figure 4).

Finally, figure 4 presents another crucial question. Are there experimental signatures of the eigenstate sequences? Clearly, a state localized in the semiclassical angle space representation need not be localized in the state space representation. However, since the quantum expectation values do pick out the sequences correctly, it is of some interest to see if there are any spectral signatures of such different classes of eigenstate sequences. Alternatively, figure 6 suggests that new modes, like the counter-rotator and local bending modes in acetylene, might appear in $SCCl_2$ due to the various bifurcations in the underlying classical phase space. Again, there must be spectral fingerprints of such new modes. More work in this direction needs to be done.

Acknowledgements

I thank Martin Gruebele and Ned Sibert for sending the full set of parameters of the fourth order effective Hamiltonian for $SCCl_2$.

References

1. See for example, (a) Lehmann K K, Scoles G and Pate B H 1994 *Annu. Rev. Phys. Chem.* **45** 241; (b) Nesbitt D J and Field R W 1996 *J. Phys. Chem.* **100** 12735; (c) Gruebele M and Bigwood R 1998 *Int. Rev. Phys. Chem.* **17** 91; (d) Keske J C and Pate B H 2000 *Annu. Rev. Phys. Chem.* **51** 323
2. Bäck A, Nordholm S and Nyman G 2004 *J. Phys. Chem. A* **108** 8782
3. (a) Jacobson M P, Jung C, Taylor H S and Field R W 1999 *J. Chem. Phys.* **111** 600; (b) Jung C, Mejia-Monasterio C and Taylor H S 2004 *J. Chem. Phys.* **120** 4194
4. Leitner D M and Gruebele M 2008 *Mol. Phys.* **106** 433
5. (a) Kellman M E and Tyng V 2007 *Acc. Chem. Res.* **40** 243; (b) Ezra G S 1998 *Adv. Clas. Traj. Meth.* **3** 35; (c) Davis M J 1995 *Int. Rev. Phys. Chem.* **14** 15; (d) Farantos S C, Schinke R, Guo H and Joyeux M 2009 *Chem. Rev.* **109** 4248
6. Sibert E L and Gruebele M 2006 *J. Chem. Phys.* **124** 024317
7. Strickler B and Gruebele M 2004 *Phys. Chem. Chem. Phys.* **6** 3786
8. Chowdary P D and Gruebele M 2009 *J. Chem. Phys.* **130** 024305
9. Rashev S and Moule D C 2008 *J. Chem. Phys.* **128** 091101
10. Chowdary P D and Gruebele M 2009 *J. Chem. Phys.* **130** 134310
11. Jung C, Taylor H S and Sibert E L 2006 *J. Phys. Chem. A* **110** 5317
12. Jung C and Taylor H S 2010 *J. Chem. Phys.* **132** 234303
13. Jung C and Taylor H S 2007 *J. Phys. Chem. A* **111** 3047
14. (a) Keshavamurthy S 2001 *J. Phys. Chem. A* **105** 2668; (b) Semparithi A, Charulatha V and Keshavamurthy S 2003 *J. Chem. Phys.* **118** 1146; (c) Semparithi A and Keshavamurthy S 2003 *Phys. Chem. Chem. Phys.* **5** 5051
15. Semparithi A and Keshavamurthy S 2004 *Chem. Phys. Lett.* **395** 327
16. Manikandan P, Semparithi A and Keshavamurthy S 2009 *J. Phys. Chem. A* **113** 1717
17. (a) Peres A 1984 *Phys. Rev. A* **30** 504; (b) Eckhardt B, Fishman S, Keating J, Agam O, Main J and Müller K 1995 *Phys. Rev. E* **52** 5893; (c) Mehlig B, Müller K and Eckhardt B 1999 *Phys. Rev. E* **59** 5272; (d) Boosé D and Main J 1999 *Phys. Rev. E* **60** 2831
18. Gruebele M 1996 *J. Phys. Chem.* **100** 12178
19. Keshavamurthy S 2007 *Int. Rev. Phys. Chem.* **26** 521